JOURNAL OF MATERIALS SCIENCE 27 (1992) 1827–1841

Characterization of graphite–aluminium composites using analytical electron microscopy

G. J. C. CARPENTER, S. H. J. LO
Metals Technology Laboratories/CANMET, Energy, Mines and Resources Canada, 568 Booth Street, Ottawa, Canada K1A 0G1

Exposure of graphite fibre/aluminium composites to elevated temperatures, such as those used for processing, can lead to degradation of the mechanical properties. Analytical electron microscopy has been used to examine the phases formed during the heat treatment of the following materials: (a) wire tows of AA6061 aluminium, reinforced with TiB_x-coated fibres, and (b) bulk composites produced by hot pressing the tows within a cladding of AA6061. In the tow material, relatively little interaction between the fibres and matrix was observed. Precipitation at the fibre/matrix interface was considerably more advanced in the as-processed bulk composite. Heat-treating both materials at temperatures in the range 580–700 °C resulted in increasingly severe interfacial reactions. Generally, the microstructures at the fibre/matrix interfaces were considerably more complex than reported in previous work. The following phases have been identified following processing or heat-treatment: Al_4C_3, α′FeSiAl, magnesium spinel, elemental silicon, $TiAl_3$, MgO, βFeSiAl and a "quarternary phase", MgSiAl(NiCu), together with amorphous oxides and porosity.

1. Introduction

Most of the current techniques developed for the fabrication of graphite/aluminium (Gr/Al) composites, such as liquid infiltration of graphite fibres with aluminium alloys [1] or hot pressing of graphite fibres with aluminium [2–4], involve processing at elevated temperatures (600–700 °C). Unfortunately, at these processing temperatures, it was found that degradation of the mechanical properties of the composites was induced. In essence, at elevated temperatures, nuclei of interfacial products are formed which subsequently grow in the fabrication stage, causing losses of both strength and ductility.

Many workers [4–17] have studied the effects of interfacial reactions, induced by thermal treatments, on the mechanical properties of Gr/Al composites. Their general conclusion is that carbon reacts with aluminium to form aluminium carbide (Al_4C_3), which nucleates on the fibre surfaces and induces degradation of the mechanical properties. Typically, a decrease of 50% or more of the as-fabricated ultimate tensile strength (UTS) was measured when the composites were subjected to thermal treatments at around 600 °C [9, 11].

In a diffusion study by Khan [9], it was concluded that carbon, because of its smaller atomic volume, diffused readily into aluminium to form Al_4C_3. Also, Shorshorov *et al.* [10] and Blankenburg [7] reported that aluminium carbide platelets on the graphite fibre surfaces appeared to grow into the aluminium matrix during the early stages of growth. Later, as the carbide platelets were about to coalesce, they penetrated the carbon fibres. The decrease in tensile strength was ascribed to stress concentrations at the notches induced by the growth of the carbide crystals into the fibres. A similar argument was presented by Khan [9], who studied the growth of the Al_4C_3 reaction zone as a function of heat treatment. He suggested that carbide particles nucleated on the fibre surfaces, increasing in size and number with increasing time or temperature, until they formed a continuous layer at the interface. This layer could be extremely irregular due to the relatively large size and random orientation of the particles. The resulting random notching of the fibre surfaces, was thought to cause drastic degradation of the fibre strength and hence of the composite strength. In contrast, Chen and Hu [18] considered that rod-like aluminium carbide nucleated from the carbon fibre and grew into the aluminium matrix, resulting in both mechanical and chemical strengthening of the interfacial bonding. They concluded that cracks propagated more easily through the interface, thereby degrading the mechanical properties. In summary, most of the authors of previous studies agreed that the tensile degradation of Gr/Al composites following thermal exposure, was caused by the formation of Al_4C_3 at the Gr/Al interfaces, although there is clearly some uncertainty regarding the precise mechanism.

In order to provide some protection against excessive formation of interfacial products at elevated temperatures and to promote wetting between

0022–2461

graphite and aluminium, a titanium–boron coating (TiB_x) is often applied to the graphite fibres [19]. This TiB_x coating is applied by a chemical vapour deposition (CVD) process from $TiCl_4$ and BCl_3 with zinc vapour used as reducing agent at a temperature of 700 °C.

Most of the earlier work [4–17] has focused primarily on the formation of Al_4C_3 as the interfacial reaction product. In many cases, the characterization of microstructure has clearly been impeded by the difficulty in preparing specimens for transmission electron microscopy. The purpose of the current work was to provide a detailed characterization of most second-phase particles present at the fibre interfaces and within the matrix phase for composites made up of TiB_x-coated fibres in a matrix of AA6061 aluminium alloy. Some of the phases at the Gr/Al interfaces described here have also been reported to some extent in the literature in previous studies on Gr/Al, specifically; the Al_4C_3 phase [7, 8, 10, 20, 21], aluminium oxide [22, 23], undetermined FeSiAl intermetallics [29] and some undetermined Al/B/C compounds [25], not found here.

The effects of thermal exposure on the microstructures of these composites have also been investigated. This work supplements the results of a more general study [26] of the effects of heat treatment on the fracture behaviour and growth of interfacial reaction products on Gr/Al composites, where only preliminary details of the TEM work were available. Because of the complexity of the microstructures and the occurrence of some second-phase particles under different heat-treatment conditions, details of their characterization have been summarized in the form of an appendix.

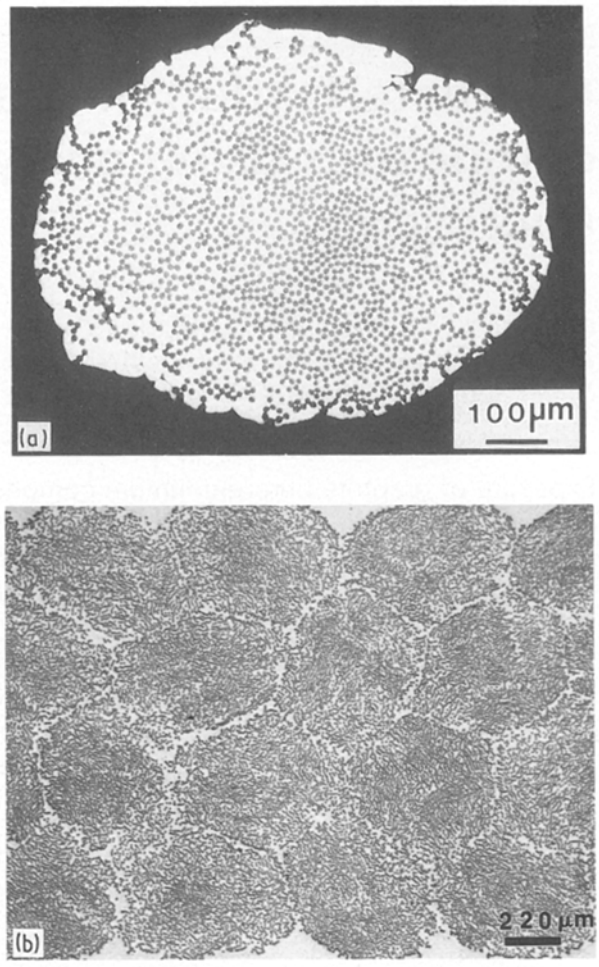

Figure 1 Optical micrographs showing cross-sections of (a) tow wire, (b) bulk composite.

2. Experimental procedure

In the present work, unidirectional graphite/aluminium (Gr/Al) composites were produced from Gr/Al precursor tows (wires). The tows consisted of AA6061 aluminium alloy reinforced with Arco pitch-based P100 graphite fibres. The nominal composition (wt %) for the AA6061 alloy is: Al–1 Mg–0.6 Si–0.28 Cu–0.2 Cr.

The fabrication procedure for the Gr/Al composite specimens in this study consisted of two stages. The first stage involved the preparation of laminates from unidirectional Gr/Al precursor tows in which sheets of tows were aligned with the same orientation and held with a polymer binder. The second stage involved hot pressing of four-layer laminates prepared from these sheets of aligned precursor wires. The conditions for the pressing operation were chosen as 13.8 MPa and 600 °C for a period of 0.5 h. These conditions were chosen to optimize compaction while minimizing (a) pressure, to reduce fibre breakage, and (b) temperature, to minimize the formation of aluminium carbide. Cross-sections of the tow and bulk materials are shown in the optical micrographs (Fig. 1).

Thermal treatments were given to both tow and bulk materials. For tow materials, the annealing temperatures of 580 and 600 °C were chosen as the temperatures typically used for hot pressing Gr/Al tows to form Gr/Al composites. In the case of the bulk Gr/Al composite, annealing temperatures up to 700 °C were used to develop more fully the reaction products at the Gr/Al interfaces.

Specimens of the tow material were prepared for TEM in two ways. Longitudinal specimens were made by embedding samples, 2 mm long, in a hole of slightly greater diameter in 3 mm discs of aluminium, ~ 0.5 mm thick, using a conducting epoxy compound. For cross-sections, seven segments of tow were embedded in an aluminium tube, 3 mm diameter, with conducting epoxy cement, and slices, ~ 0.5 mm thick, were cut using a diamond saw. Samples from the bulk composite were cut in the same manner and 3 mm discs were removed by means of a spark machine. The discs were ground to a thickness of ~ 120 μm and dimpled mechanically from both surfaces with diamond paste in a Gatan Dimpler Grinder to a central thickness of ~ 40 μm. Final perforation was carried out by argon-ion sputtering at 5 keV in an Ion Tech thinning apparatus at an incident angle of 12–15° at room temperature. Although some heating of the specimens was expected during sputtering, the fact that widely different microstructures were observed in the aluminium alloy matrix from the different specimens is evidence that this effect and possible damage from dimpling, were of minor importance for the materials examined.

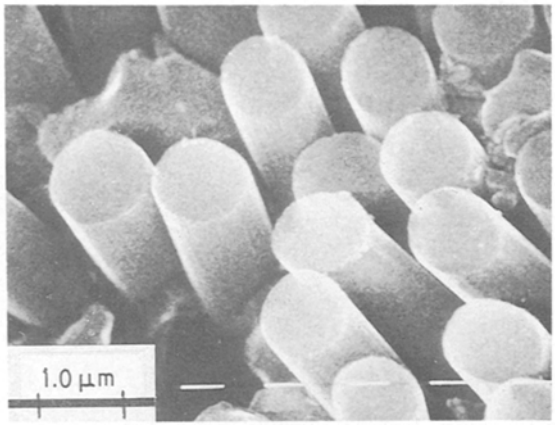

Figure 2 Scanning electron micrograph, showing graphite fibres that had been pushed out of the matrix during thin foil preparation as a result of the grinding operation: tow material, annealed 2 h at 600 °C.

Some difficulty was found in preparing cross-sectional specimens because the pressure during the grinding operation tended to push the graphite fibres down into the thermal-setting wax used to hold them on the grinding rig. An example of this is shown in Fig. 2. This effect was particularly noticeable with specimens that had been annealed. This provides a clear indication that the fibres were often either weakly bonded or not bound at all to the matrix phase. The result of having fibres standing proud of the matrix in some specimens meant that it was not always possible to produce cross-sections where both the graphite and the matrix were transparent to electrons at the fibre/matrix interfaces. The effect could be minimized by dimpling the specimen on one side only, so that only a very thin layer of wax was needed to hold the flat specimen surface in contact with the mounting surface of the dimpler.

The specimens were examined in a Philips EM 400T TEM/STEM, operated at 120 kV and fitted with an Edax 9100/60 EDS system for X-ray (EDX) analysis and a Gatan (model 607) electron energy loss spectrometer (EELS) for light element analysis. The EDX system was calibrated for quantitative elemental analysis using various standards. However, it must be recognized that because of the presence of the mainly aluminium matrix, which will result in a low level, spurious signal from the entire specimen, as summarized by Williams [27], it is not possible to specify the aluminium concentration in the precipitate particles in a fully quantitative manner. Some specimens were also examined at the National Research Council Laboratories, Ottawa, in a Philips EM 430T microscope, operated at 300 kV and in a Zeiss EM 902 microscope for electron spectroscopic imaging.

3. Results

3.1. As-prepared composites

3.1.1. Tow material

Typical micrographs of the tow material are shown in Fig. 3. The carbon fibres were mainly crystalline, with a strong texture along the longitudinal direction (Fig. 3a), as expected for pitch-based fibres. The amorphous TiB_x coating could be readily distinguished, particularly in cross-section, as a dark band, 25–50 nm thick (Fig. 3b), as a result of its higher atomic number contrast and amorphous structure. The coating followed the contours of the surface of the graphite fibres although there was a tendency for it to be detached from the fibres over large areas. A similar degree of TiB_x separation can also be seen in earlier work, where a 201-type aluminium alloy was used for the matrix material [28]. This phenomenon was confirmed by the examination of very thick (many micrometres) regions of foil, where possible differential sputtering could not have created imaging artefacts. It was clear in this case that a gap (typically 100–200 nm wide) existed in many areas between the graphite fibres and the TiB_x coating. It is thought that this arose from the grinding operation used during specimen preparation, as a result of the flexing of the exposed graphite fibres, which tend to stand proud of the specimen surface, as described in Section 2. It can readily be shown that such a large gap could not have arisen from differential thermal contraction strains. Although this effect appears to be an artefact of the specimen preparation, it is clear that the bond between the fibres and the TiB_x coating is relatively weak. This contrasts with the bond between the TiB_x and the matrix, which was sufficiently strong that separation from the aluminium-alloy matrix was not normally observed. A similar conclusion was drawn from studies of the fracture characteristics of these composites [26], based on examination in a scanning electron microscope.

The aluminium-alloy matrix possessed a high density both of dislocations and of small "defect" clusters, 10–50 nm diameter (Fig. 3a). No evidence for the precipitation of alloying elements within the grains was observed. EDX analysis failed to reveal the presence of any segregated alloying elements associated with these clusters. A further check using energy-filtered imaging (which gives a higher spatial resolution, ~ 2 nm) also failed to reveal solute segregation. It is most likely that the "black spot" defects were formed as a consequence of the ion-beam implantation damage during sputtering. Similar features were not visible in any of the heat-treated specimens. It appears that the presence of alloying elements dissolved in the aluminium matrix may be necessary to stabilize the damage clusters caused by ion sputtering. The high density of network dislocations probably arose from differential thermal contraction during solidification and cooling.

No evidence for the presence of Mg_2Si precipitates was found in the tow material. Occasionally, coarse intermetallics (~ 1 μm diameter), containing mainly iron, silicon and aluminium with smaller amounts of chromium, manganese and copper, were observed at grain boundaries of the alloy matrix, including regions where a boundary intersected the TiB_x/matrix interface (see also Fig. 5a). CBED analysis showed that these precipitates were not of the type αFe_2SiAl_8, as tentatively suggested previously [26] on the basis of optical and scanning electron microscopy; the proper designation is the bcc α'FeSiAl phase, as described

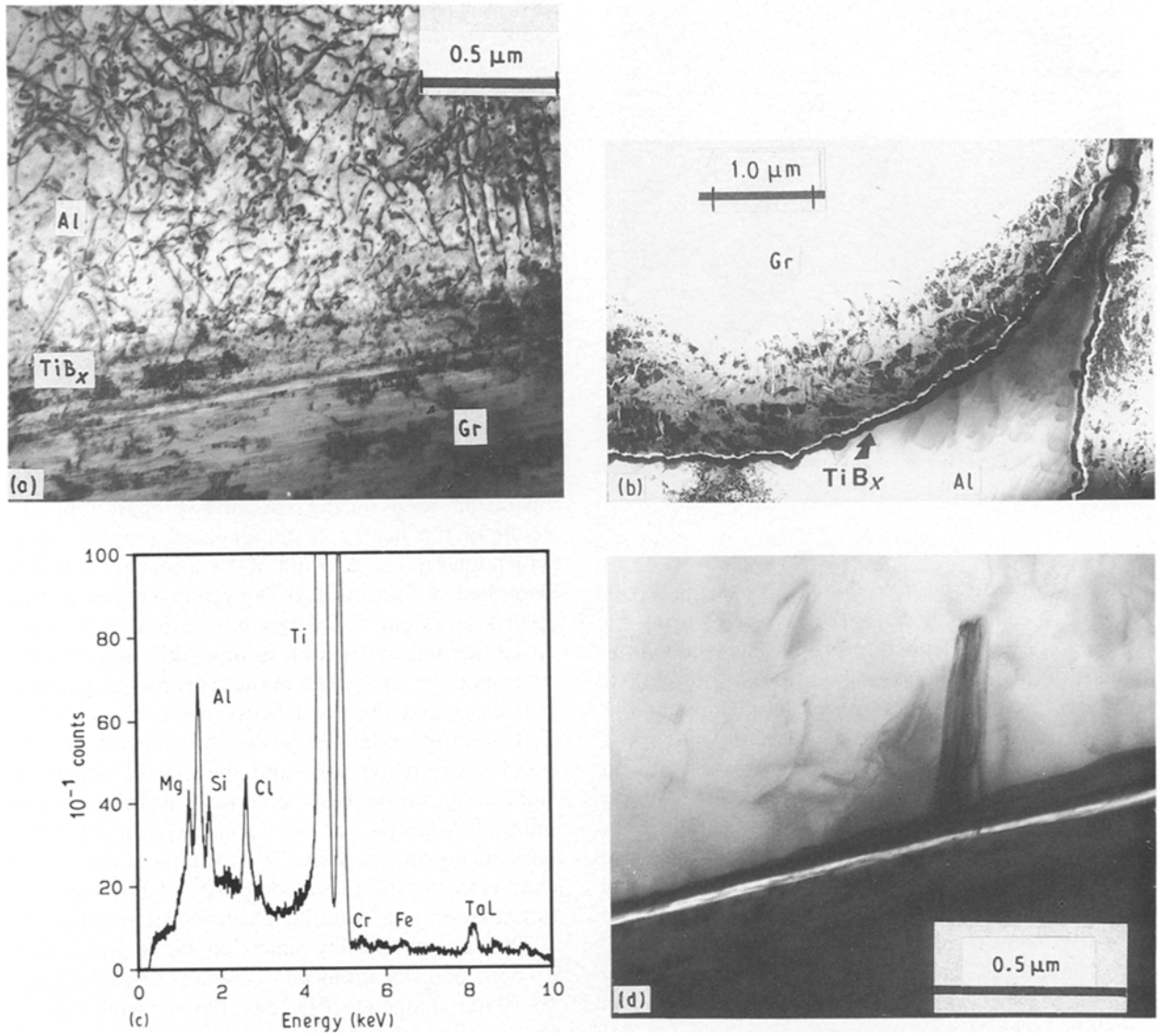

Figure 3 Features of the microstructure of the tow material. (a) Longitudinal section, showing a typical fibre/matrix interface, at which precipitation had not taken place. (b) Cross-section, showing the TiB_x layer. (c) EDX spectrum, taken with an electron beam, ~ 15 nm diameter, located on the TiB_x layer which was aligned parallel to the electron beam. (d) Longitudinal-section, showing a platelet of Al_4C_3, precipitated at the fibre/matrix interface; specimen oriented so that the dislocations were almost out of contrast.

in the Appendix. EDX analysis of precipitates that passed right through the foil gave an approximate composition of $(FeM)_2SiAl_8$, where M corresponds to (Cr + Mn + Cu) at a total concentration of ~ 3%.

EDX analysis of the TiB_x interlayer, in addition to showing titanium, indicated the presence of chlorine, which probably arose from the chemical vapour deposition process used to lay down the fibre coating. In addition, the principal alloying elements from the aluminium alloy had segregated to a limited extent into the TiB_x interlayer. Fig. 3c shows that magnesium and silicon were particularly prominent, with minor quantities of chromium and iron also being present. It was difficult to ascertain whether aluminium was present in the TiB_x, because of interference from the aluminium-alloy matrix. Analyses from thin areas, using an electron probe size of ~ 15 nm, indicated that these elements were present throughout the thickness of the TiB_x layer. Spectra obtained with the electron beam straddling the boride/matrix interface indicated a greater concentration of the segregated elements in such regions, although further work with a finer probe size (such as that in a dedicated STEM) would be desirable to confirm this observation. Analyses taken within the matrix showed no evidence for the presence of these segregated elements at distances as close as 50 nm to the TiB_x. The only element present in the graphite phase that showed up using EDX analysis was argon, which had become incorporated during ion-beam thinning.

Although the fibre/matrix interfaces were mainly free from second phases, precipitates were occasionally visible, growing into the aluminium-alloy matrix from the TiB_x interface (Fig. 3d). EDX analysis from these precipitates revealed only the presence of aluminium, indicative of the carbide phase Al_4C_3, that results from the interaction between fibre and matrix [4–17]. This was confirmed using convergent beam electron diffraction (CBED). Tilting experiments showed that although these carbides sometimes had the appearance of rods [18] they actually took the form of platelets that were typically 50 nm thick by

500 nm diameter. Occasionally, equiaxed intermetallic precipitates (50–300 nm diameter), shown by EDX and CBED analysis to be composed of the α′FeSiAl phase, as described above, were present at the TiB_x/matrix interface.

3.1.2. Bulk composite

The additional heating cycle to which the tow material was subjected during its conversion to a bulk composite had resulted in significant changes to the microstructure. Although the dislocation structure of the matrix was largely unchanged and the "black spot" defects were still present, many precipitates of the b c c phase, α′FeSiAl (see Appendix), were observed in the matrix (Fig. 4a). These precipitates differed from the large α′ particles seen at the grain boundaries and TiB_x interfaces in that they contained relatively high concentrations of chromium. EDX analysis gave an approximate composition of $FeCrSi_2Al_{10}$. As noted in Section 2, the principal uncertainty in this analysis is for the aluminium concentration. The particles were elongated, with an aspect ratio of approximately 2:1, having sizes typically in the range 25 nm × 50 nm to 50 nm × 100 nm and were present at a concentration estimated to be $\sim 2 \times 10^{19}\,m^{-3}$. Comparison with a published EDX spectrum indicates that these precipitates probably correspond to the "cuboidal" phase observed in a similar composite by Allard *et al.* [29]. Occasional observations of the high-chromium α′-phase were also made at grain boundaries in the matrix.

Precipitation at the matrix/TiB_x interface was considerably more advanced than in the tow material (Fig. 4a). In some regions of foil, up to 50% of the interface contained precipitates. Because the Al_4C_3 particles were slightly larger and more numerous than in the tow, it was possible to confirm that they always took the form of platelets, in common with the morphology of the much larger particles observed using the SEM [26] and by TEM, in samples that had been annealed. The platelets had an aspect ratio of ~ 7:1 and were typically in the size range 15 nm × 100 nm to 45 nm × 300 nm.

Intermetallics that were approximately equiaxed with diameters in the range 0.2–1 μm, were also present at the interface in approximately equal density to the carbides. These intermetallics were also shown by

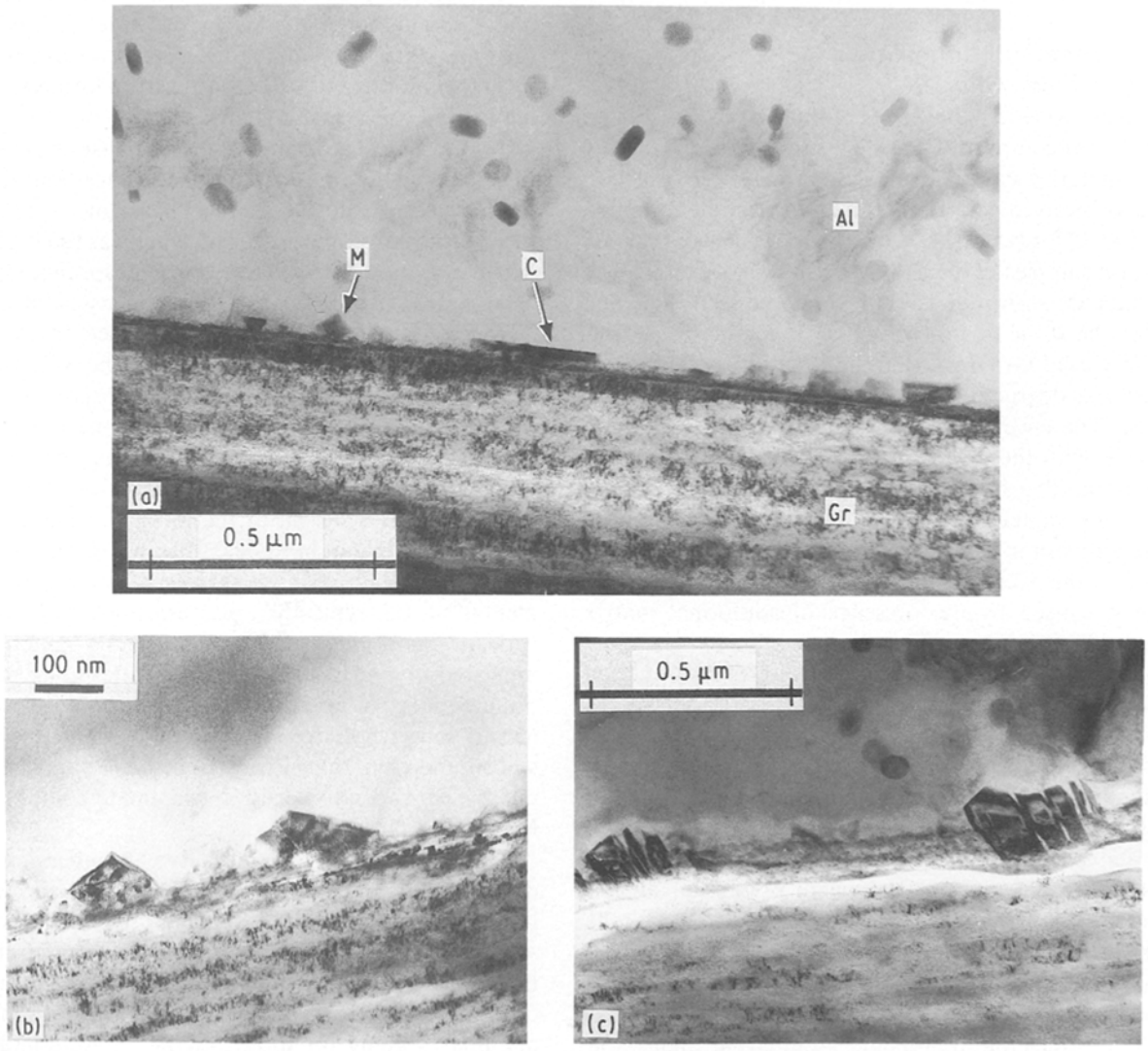

Figure 4 Transmission micrographs of specimens prepared from the bulk composite (a) showing the presence of α′FeSiAl intermetallic particles in the matrix and various precipitates at the fibre/matrix interface, M = Mg spinel, C = Al_4C_3; (b) an interfacial precipitates identified as magnesium spinel, (c) precipitates of elemental silicon at the fibre/matrix interface.

CBED analysis to be the α′FeSiAl phase and appear to correspond to the "large" or "lathe-shaped" precipitates reported by Allard *et al.* [29]. EDX analysis showed that they had a similar composition to the large, low-chromium α′ particles observed in the tow material. Similar precipitates were also observed at the grain boundaries.

Angular precipitates, 50–300 nm diameter, that showed only magnesium and aluminium in EDX spectra, were a prominent feature at the fibre/matrix interfaces (Fig. 4b). They were shown to be the magnesium spinel ($MgAl_2O_4$), as described in the Appendix. Also, twinned precipitates, 100–500 nm diameter, composed of elemental silicon (Fig. 4c), were sometimes present at the interface (see Appendix). Occasional observations were made of the "quaternary" MgSiAl(NiCu) phase at the fibre/matrix interfaces. In some interfacial regions, clusters of these various precipitates were present, having nucleated in the same area. In regions of the interface that were free from precipitation, no evidence for gradients of solute concentration in the matrix phase could be discerned using EDX analysis. However, some segregation of the alloying elements to the TiB_x interlayer was apparent, as described for the tow material.

3.2. Effects of annealing

3.2.1. Tow material

In order to assess the effects of thermal treatments on the Gr/Al composites, tensile testing of the as-received tow material was performed. Specimens were tested in the as-received condition and after being heat-treated at 600 °C for 0.5 or 2 h. In addition, tests were carried out on samples of the as-processed bulk material. The results are shown in Table I. It can be seen that even after the 0.5 h treatment, which is a condition commonly used for converting the tows into a bulk composite, a degradation in strength of 13% was measured. The effect of the 2 h heat treatment was more severe, with the tow losing more than one-third of its strength. The hot-pressing operation used to create the bulk material also resulted in a reduced tensile strength, but in this case the interpretation is complicated by the overall reduction in volume fraction of the fibres, caused by the presence of additional matrix material.

Specimens for TEM were prepared from samples of precursor tow, annealed for 2 h at 580 and 600 °C. Intermetallic particles, 100–500 nm diameter, composed of the α′FeCrSiAl phase, were present in the aluminium alloy matrix in the specimen annealed at 580 °C, comparable with the as-prepared bulk composite, but were less commonly observed after the 600 °C anneal. Dislocations were present in all annealed samples, with some tendency towards the formation of cells, ~ 5 μm diameter. The black spot defect clusters, present in the tow and composite samples were not observed.

The annealing treatments resulted in significant changes at the graphite/matrix interfaces. A typical montage from a cross-sectional specimen, annealed at 580 °C (Fig. 5), shows several features of the microstructure, including (a) the α′FeCrSiAl precipitates present in the matrix, (b) α′ and βFeSiAl intermetallics (~ 1 μm diameter) nucleated at the fibre/matrix interfaces, (c) a precipitate of $TiAl_3$ (~ 1 μm diameter), in this case, formed in association with a particle of the α′FeSiAl phase, (d) a large (~ 2 μm diameter) α′FeSiAl intermetallic, grown at an interface/matrix/grain boundary intersection, (e) a reaction zone (~ 1 μm wide, shown at a higher magnification in Fig. 5b) that consisted of MgO (periclase) crystals in a porous amorphous matrix, that appeared to be composed of an aluminium-rich oxide, and (f) fine-scale (~ 100 nm diameter) precipitates of Al_4C_3, sometimes in the form of discontinuous layers at the fibre/matrix interface. The preferred nucleation of second phases (most commonly Al_4C_3 or FeSiAl intermetallics) at the fibre/matrix/fibre junctions were also seen; Fig. 5a shows an example of a βFeSiAl particle formed in this manner.

TABLE I Tensile strength of the Gr/Al composites

Specimen	Condition	UTS (GPa)
Tow	As-received	1.3 ± 0.06
Tow	1/2 h, 600 °C	1.13 ± 0.20
Tow	2 h, 600 °C	0.83 ± 0.15
Bulk	Hot-pressed, 1/2 h, 600 °C	0.90 ± 0.10

Two types of FeSiAl intermetallic phases were identified at the fibre/matrix interfaces. One was the α′ phase, having a low chromium content (~ 1%), as seen in the bulk composite. The other was the β-phase, which was not detected in the bulk specimens; the crystal structure of this phase was reassessed as B-face centred orthorhombic, as described in the Appendix. Because of the complexity of the microstructure, a detailed survey of the relative proportions and distribution of these two intermetallic phases was not carried out, although it may be noted that the β-phase was detected primarily at fibre/matrix/fibre junctions.

Other phases present at the interface regions after this heat treatment, but not visible in Fig. 5a, were (a) large platelets of Al_4C_3 (~ 1 μm diameter), (b) elemental silicon, typically ~ 0.5 μm thick by ~ 2 μm wide, (c) porous crystalline/amorphous zones that appeared to consist of $TiAl_3$ precipitates in an amorphous matrix of an Al/Si oxide and, in a few cases, (d) an intermetallic containing mainly magnesium, silicon and iron, that was identified as "quarternary" phase (see Appendix), with approximate composition $Mg_3Si_6Al_9(Ni_{0.65}Cu_{0.35})$.

A rough survey of the relative numbers of the different constituents over a large area of specimen, indicated approximately equal numbers of the large Al_4C_3 particles and FeSiAl intermetallics, and about half as many $TiAl_3$ and silicon precipitates, with the crystalline/amorphous reaction zones and quarternary phases being (in total) on the < 10% level. It should be noted that although Fig. 5a gives a clear indication of the general manner in which precipitation had taken place, the representation of the large

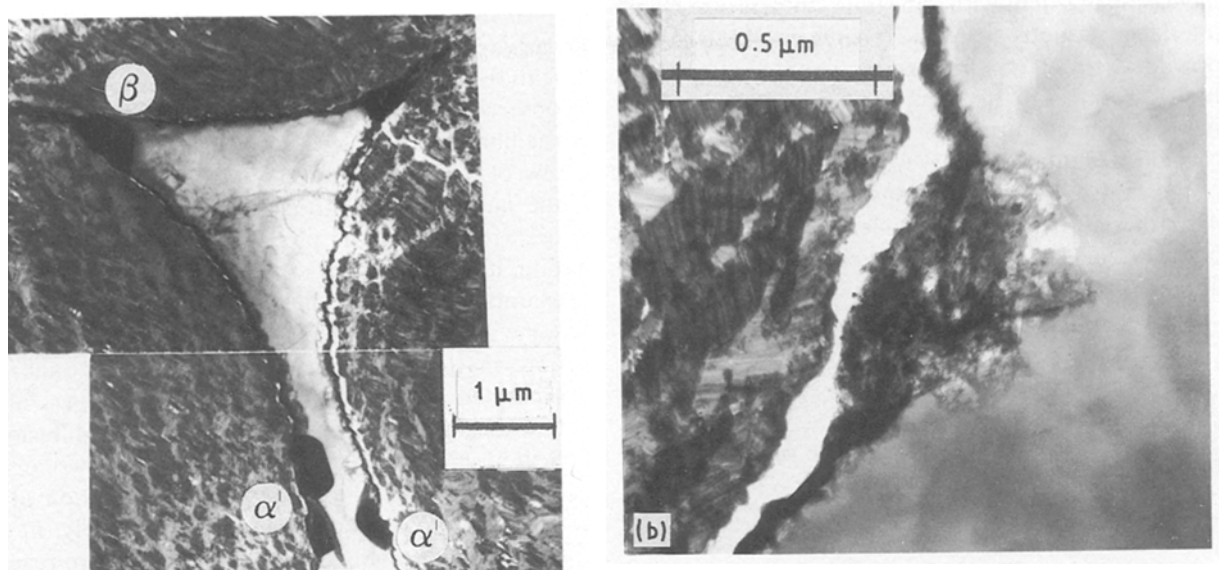

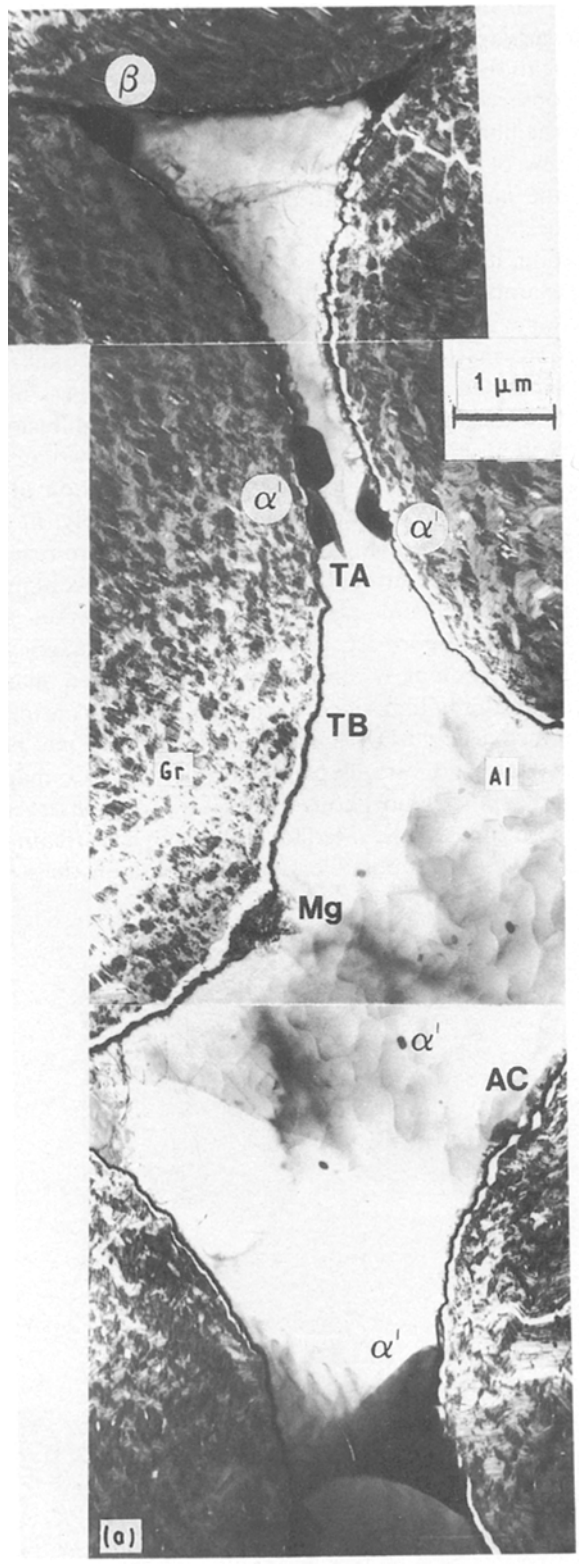

Figure 5 Micrographs from tow material, following heat treatment. (a) Montage of a cross-section, after annealing for 2 h at 580 °C. (b) Enlarged region composed of MgO precipitates in an amorphous reaction zone ("Mg" from (a)). Gr, graphite fibre; Al, AA6061 matrix; α',β, FeSiAl; TB, TiB_x; TA, $TiAl_3$; Mg, magnesium-rich zone; AC, Al_4C_3.

Al_4C_3 platelets at the interfaces was less than average in this field of the thin foil.

The thickness of the TiB_x layer was revealed by tilting the sample until the interlayer was in the "end-on" orientation, showing it to have thickened to 50–70 nm as a result of the annealing treatment. Presumably this is caused by increased porosity in the layer, resulting from reactions during heat treatment.

The 600 °C treatment resulted in more extended reactions at the fibre/matrix interfaces of the tow specimens compared to the 580 °C anneal. Cross-sections revealed porous reaction zones up to ~ 1 μm wide that sometimes extended up to many micrometres around the fibres. Although the reaction zones were not all identical, most had certain common characteristics: (a) a high degree of porosity, (b) the presence of aluminium, silicon, oxygen, often carbon, and at low levels, the alloying elements chromium, iron and copper, and (c) being composed of mixed crystalline and amorphous phases. Remnants of the TiB_x layer were frequently visible, straddled, in some cases, by the reaction zones, which often contained aluminium, silicon and magnesium or aluminium, silicon and titanium. These regions appeared to be similar in character to those observed in the 580 °C specimen, but much more extensive.

3.2.2. Bulk composite

Heat treating the bulk composite for 2 h at 600, 650 and 700 °C resulted in major changes in the microstructure that increased in severity with temperature. The aluminium-alloy matrix phase typically contained dislocation cells or subgrains, 1–5 μm diameter. A low density of coarse FeSiAl intermetallics (200–500 nm diameter) was present in the matrix after the 600 °C anneal (Fig. 6a) and the density decreased with increasing temperature. These precipitates had been tentatively identified as the αFeSiAl phase in our earlier paper [26], based on EDX data. However, a definitive analysis using CBED has shown these particles to be of the type α'FeSiAl. EDX analysis showed that this intermetallic possessed a composition of approximately $Fe_2CrSi_2Al_{18}$. These coarser particles contained a lower chromium concentration than the matrix precipitates in the as-processed bulk composite.

The reactions at the fibre/matrix interfaces were essentially similar to those seen with the tow material,

increasing in extent with annealing temperature. Some interfacial regions were fairly uniform, with Al_4C_3 precipitates and, less frequently, α′FeSiAl intermetallics, growing into the matrix phase. However, with increasing temperature, the size and concentration of carbide precipitates increased, together with the extent of the oxidized crystalline/amorphous reaction zones. Also, there was increasing evidence for the growth of both carbides and the reaction zones into the graphite fibres.

In the samples annealed at 650 and 700 °C, large carbides (1–5 μm diameter, Fig. 6b) were a major feature of the microstructure and some were also observed within the aluminium matrix, distinct from the fibre–matrix interfaces. Whilst it is possible that a few of these observations may have been caused by the nucleation of particles on an interface that had been lost during the preparation of the thin foil section, it is unlikely that this would account for all the examples observed. It is therefore concluded that some of these platelets had either nucleated at a fibre–matrix interface and, being loosely bound, had separated into the molten aluminium, or (less likely) that they had nucleated as a result of the diffusion of carbon into the liquid phase.

The extent of the reactions and oxidation at the fibre/matrix interfaces varied considerably in any given specimen (Fig. 6c–e). The most severe reaction regions were irregular, extended zones containing amorphous and crystalline regions, together with substantial porosity. These zones were sometimes extremely complex, containing carbon, oxygen, magnesium, aluminium, silicon, titanium and chlorine (determined using EDX analysis and EELS). Fine $TiAl_3$ crystals and various combinations of MgO, magnesium spinel, amorphous oxides, etc., were observed in these zones at the interfaces following heat treatment. Whilst it is not possible to assess accurately the size of

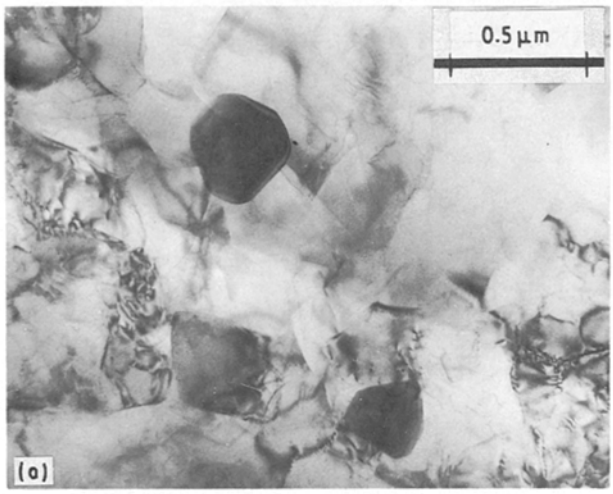

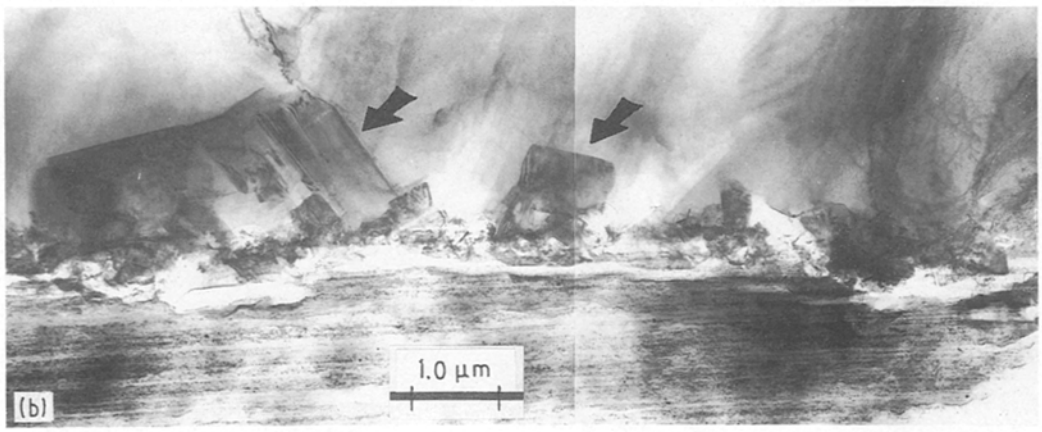

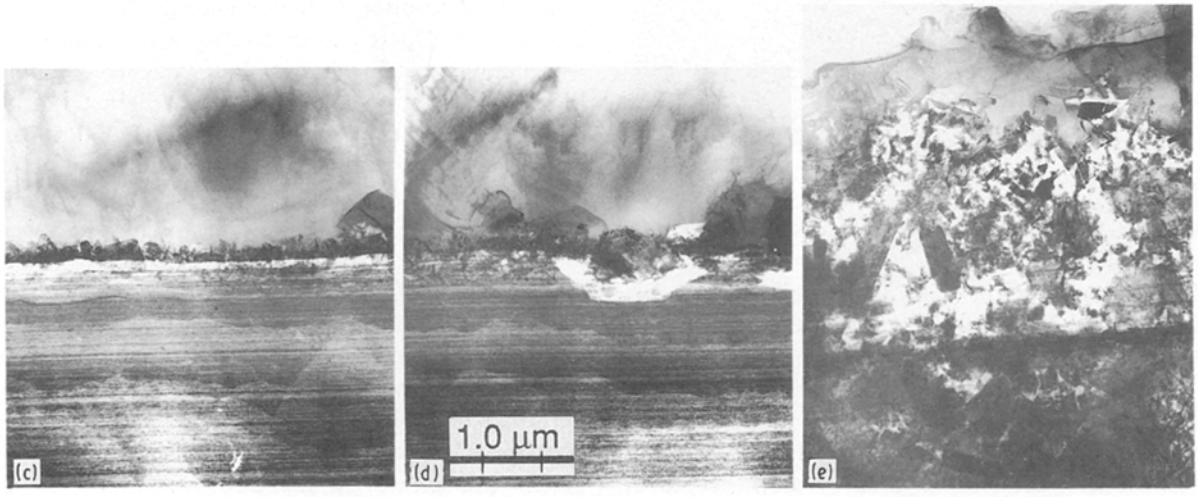

Figure 6 Microstructures from bulk composite material, after heat treatment for (a) 2 h at 600 °C, dislocation sub-grains and α′FeSiAl intermetallics in the aluminium alloy matrix, (b) 2 h at 700 °C, showing precipitated Al_4C_3 at a fibre/matrix interface, (c–e) 2 h at 700 °C, showing varying degrees of interaction at the fibre/matrix interfaces.

such regions from TEM, one such zone measured about 25 μm by 2 μm in a thin foil from a longitudinal sample, heat treated at 700 °C. Because of the limited volume sampled in a thin foil, it would be expected that very much larger zones would be present in practice.

The TiB_x interlayer was not readily discerned in many areas of these specimens. Even when this layer was still apparently intact, substantial precipitation had occurred at the interface with the matrix. In regions of the interface where the TiB_x layer was not readily defined, EDX analysis showed the presence of titanium in most cases. It is possible that mixed amorphous oxides containing titanium were present in addition to the $TiAl_3$ crystals that were often observed; however, it has not been possible to demonstrate this unambiguously because of overlap effects. In addition to the fine $TiAl_3$ crystals that were present in oxidized reaction zones, larger crystal (~ 0.5 μm diameter) were sometimes present at the interface, similar to those observed in the tow material after annealing.

4. Discussion

We have shown that the microstructures produced in $Gr/TiB_x/Al$ composites by high-temperature processing or heat treatment can be extremely complex. Because of this, it was considered useful to indicate the phases formed in the simplified sketches, as shown in Fig. 7. In referring to these, it must be recognized that they are highly schematic and that widely varying microstructures were in fact observed in different areas of the heat-treated specimens. Although Al_4C_3 was observed to varying degrees at the fibre/matrix interfaces in all specimens, no evidence was obtained for the Al/B/C [25] or Al/C/O phases [28] reported elsewhere.

Although a surprisingly large number of phases were observed in these composites, no evidence was obtained for the presence of Mg_2Si in the matrix or at the fibre/matrix interface, although it is normally the primary strengthening phase in AA6061 alloys. It appears that this is a consequence of the segregation of magnesium to the fibre/matrix interfaces, which upsets the balance of magnesium and silicon needed to cause precipitation of the binary phase. Instead, the excess silicon either remains in solution or precipitates mainly in the form of the α'FeSiAl phase that was a prominent feature of many of the specimens; less commonly, silicon may also precipitate as elemental silicon, βFeSiAl or in the form of the quarternary phase. The simultaneous appearance of these various phases in the same specimen is probably a consequence of variations in chemistry that come from the heterogeneous nature of a composite material.

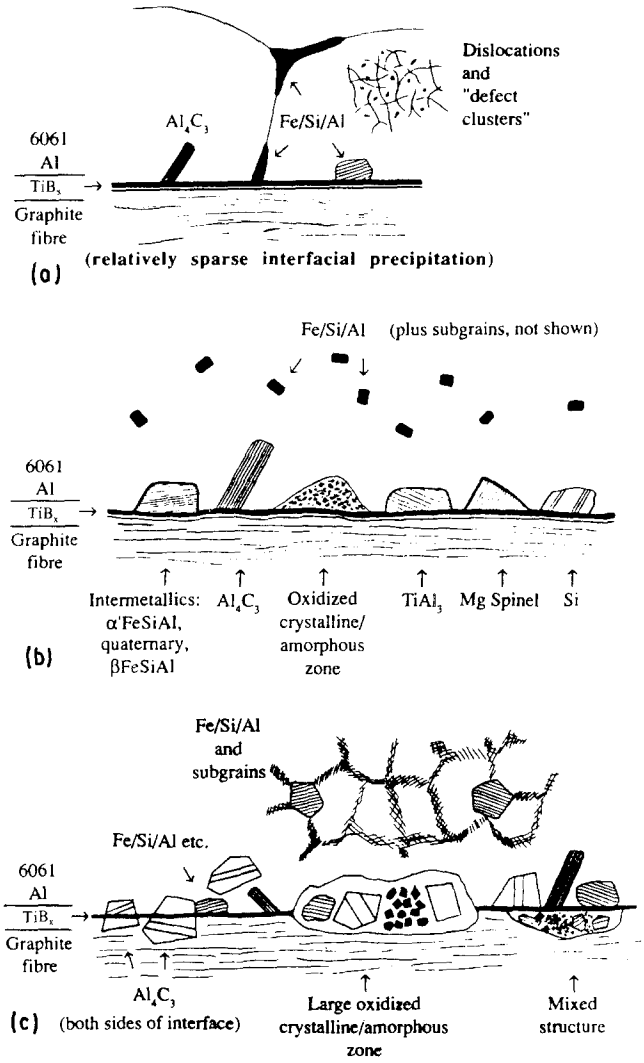

Figure 7 Schematic diagrams, illustrating the phases and microstructures observed in the composite specimens: (a) as-received tow; (b) intermediate temperature heat treatments (580–600 °C) and bulk composite; (c) high-temperature heat treatments (650–700 °C).

It is interesting to compare the effects of thermal treatment on the interfacial characteristics of Gr/TiB_x/Al composites (i.e. graphite fibres with a TiB_x coating) and of Gr/Al without a TiB_x coating [4–17]. In this study, the interfaces of the Gr/TiB_x/Al tow, in the as-received condition, were relatively free from second phases, containing only occasional particles of Al_4C_3 and α′FeSiAl on the matrix side of the Al/TiB_x interface.

After heat-treating the composites, additional phases such as $TiAl_3$, $MgAl_2O_4$, Si, quaternary MgSiAl(CuNi), MgO, amorphous oxides, and βFeSiAl were observed at the Gr/TiB_x/Al interfaces. The two major effects of increasing the heat-treatment temperature were to enhance both the formation of carbide platelets and the reactions at the interface involving oxidation. The carbide platelets were found to grow primarily into the aluminium matrix from the TiB_x interface at the lower temperatures. However, with the higher temperature treatments (600–700 °C), the carbide platelets and oxidized zones were found on both sides of the TiB_x interlayer. The carbides were also seen, to a limited extent, isolated in the aluminium matrix.

The lack of an orientation relationship between the carbides at the TiB_x/Al interfaces (described in the Appendix) and the aluminium matrix was also reported by Chen and Hu [18]. It appears that the solidification front during cooling moves from the aluminium liquid towards the fibres, thus precluding the possibility of solid aluminium nucleating on the carbides with a preferred orientation. It is unlikely that the carbide precipitates form in any preferred orientation relative to the textured graphite fibres unless a breakdown of the amorphous TiB_x barrier layer is a pre-requisite for carbide nucleation. No evidence for this has been observed, so that it appears that carbide precipitation in the aluminium matrix occurs by the diffusion of carbon through the TiB_x barrier layer. This raises the question whether a crystalline TiB_x interlayer would be more resistant to the diffusion of carbon than a vapour-deposited amorphous layer, which effectively contains a high potential for enhanced diffusion through the large (effective) concentration of defects present. The film of TiB_x clearly did not prevent the growth of carbides into both the graphite fibres and the matrix phase at high enough temperatures and the deleterious effects of carbides in Gr/Al composites were also found in the Gr/TiB_x/Al composites. For example, the tensile tests have shown decreases in ultimate tensile strength of more than one-third in tows heat treated for 2 h at 600 °C.

It is clear that heat-treatment of these composites in air at elevated temperatures leads to substantial ingress of oxygen and the formation of various oxide phases and, probably, to the presence of significant porosity. Atmospheric oxygen and moisture are the most likely sources of contamination. This may occur in two ways; through the graphite fibres themselves and down the fibre/matrix interfaces. Both may be important. It is likely that graphite fibres are readily permeated by various gases. In addition, this and other studies have shown that the bond between the carbon fibre and the TiB_x coating is relatively poor, so that it is possible that this interface forms an easy diffusion path for the ingress of atmospheric gases.

In summary, despite the fact that TiB_x forms a stronger bond with aluminium than with graphite, and that TiB_x probably helps to inhibit the formation of Al_4C_3, the deleterious effects of degradation in mechanical properties as a result of carbide formation are also found in Gr/TiB_x/Al composites.

Acknowledgements

The authors are grateful to the following for their contributions to this study: Dr D. Zimcik, Canadian Space Agency, for the supply of Gr/Al composites; M. Charest, MTL/CANMET, for technical skill in the preparation of thin foils from these composite specimens which was an essential component of the project; J. McCaffrey, National Research Council Laboratories, for help with the operation of the EM 430T electron microscope and Dr D. Downham, National Research Council Laboratories, for examination of the tow material using energy-filtered images in the Zeiss microscope.

Appendix: detailed analyses of second phases

Aluminium carbide

The aluminium carbide phase, Al_4C_3, was completely analysed using CBED and EELS. All CBED patterns could be indexed according to the rhombohedral crystal structure, using hexagonal cell coordinates, $a = 0.334$ nm and $c = 2.50$ nm. An example of a diffraction pattern from a large precipitate that passed right through the foil is shown in Fig. A1a. The carbide phase always took the form of plates, as also observed for the large (1–5 μm diameter) particles seen in SEM studies [26]. The lattice image, shown in Fig. A1b, confirms that the basal planes are parallel to the habit planes of the carbides, not perpendicular to this plane as implied in earlier work, where the particles were reported to be rod-shaped [18].

Using CBED patterns, an attempt was made to determine whether an orientation relationship existed between the aluminium matrix and the carbide phase. Three specimens were examined; a tow wire sample, a bulk composite in the as-processed condition and the same material after annealing for 2 h at 700 °C. The specimens were tilted through large angles using a calibrated double-axis tilt holder so as to reveal prominent zone axes of either matrix or carbide phases. The rotations of the image and the diffraction pattern caused by the microscope lenses were also calibrated so that it was possible to plot the zone axes, the diffracting planes and the carbide orientation on the stereographic projections. After obtaining data from two carbides from each type of specimen, it was concluded that in no case were any of the prominent planes or directions of the matrix and precipitate phases accurately parallel. A typical example is shown in Fig. A1c. Although the $(0\,0\,1)_{Al}$ and $(1\,\bar{2}\,1\,0)_{Al_4C_3}$

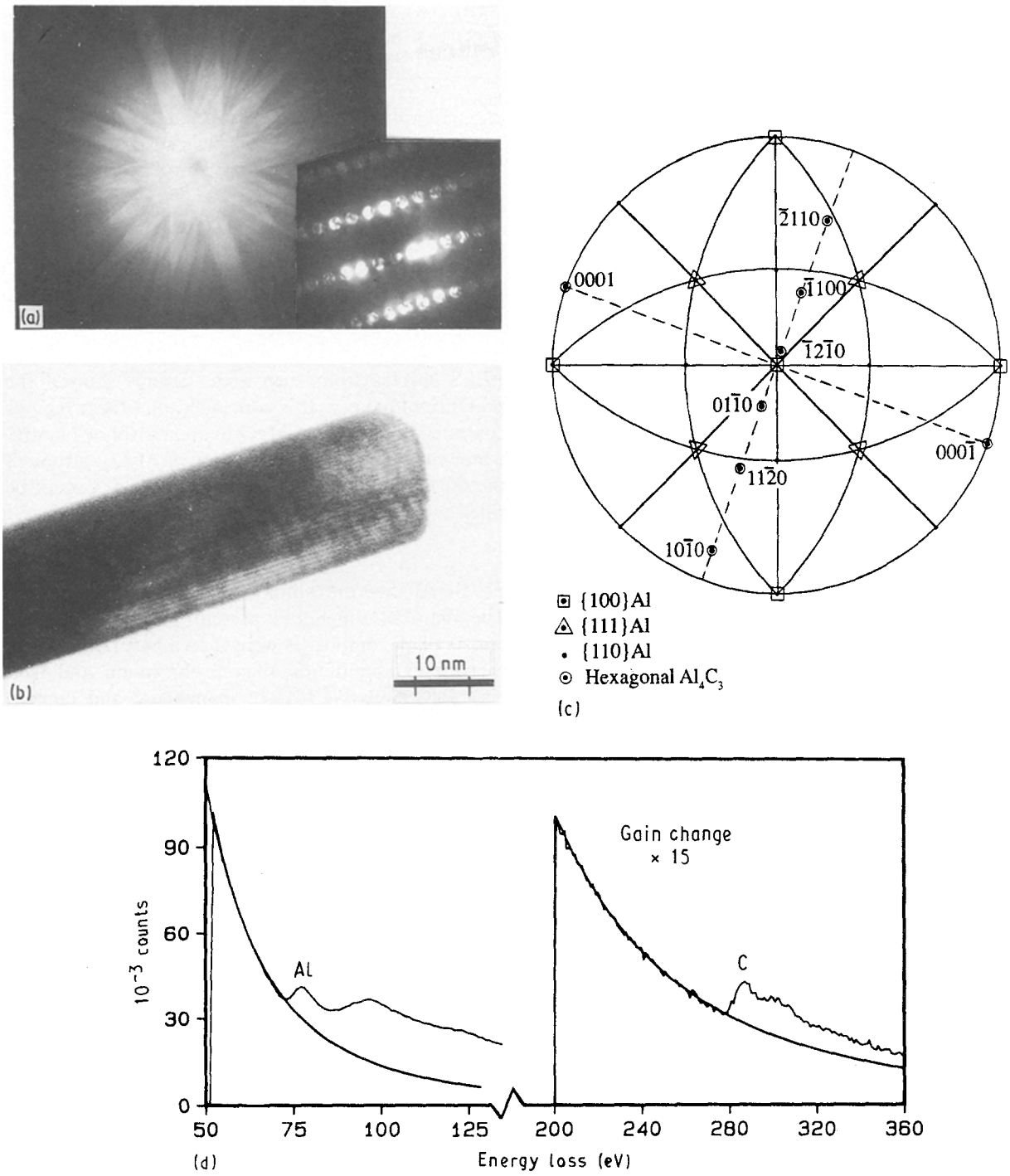

Figure A1 Identification and orientation of the Al_4C_3 phase (bulk composite, heat treated 2 h at 650 °C): (a) CBED pattern, $[1\,1\,\bar{2}\,0]$ zone axis; (b) lattice image, showing the (0 0 0 3) planes, which are parallel to the plane of the carbide platelet; (c) typical stereogram, showing the orientation of a carbide precipitated at a fibre/matrix interface, superimposed upon that of the aluminium alloy matrix; (d) EELS spectrum.

poles appear to lie close together at the centre of the projection, they are in fact separated by 8°, which is much greater than the errors of the projection (1°–2°). Furthermore, a comparison between the results from different carbides indicated that the relative orientations between carbide and matrix had no common elements and were therefore essentially random. Further confirmation of this conclusion was obtained by tilting several carbides so that the basal planes, {0 0 0 1} (close-packed {1 1 1}, in rhombohedral coordinates) were oriented parallel to the electron beam. In an orientation relationship with such a phase, it is most likely that a prominent set of matrix planes would be parallel to the basal planes of the carbide. However, in no case was a prominent matrix reflection excited when this carbide orientation was selected. Chen and Hu [18] also asserted that no orientation relationship existed between the carbides and matrix material.

Spectra obtained using EELS revealed only the presence of aluminium and carbon (Fig. A1d), in confirmation of the diffraction results. Quantitative analysis of a thin carbide that passed right through the foil using published *k*-factor data [31] yielded a composition of Al–37 at % C, in reasonable agreement with that expected for Al_4C_3 (Al–43 at % C), within

the accuracy of the data. EDX analysis did not reveal other elements segregated within the carbide phase. The carbon peak did not show up in spectra from the Al_4C_3 using an ultra-thin window EDX detector, a result of strong absorption of C*K* X-rays by the aluminium. Once a number of carbides had been identified, it was possible to conclude that facetted, plate-like precipitates that showed only aluminium in the EDX spectra (and sometimes contained twins) were always composed of the Al_4C_3 phase.

Magnesium spinel

One of the magnesium-rich phases that was observed both in the as-prepared bulk composite and in the heat-treated tow material was identified as magnesium spinel. A typical example is given in Fig. 4b and a single-crystal CBED pattern is shown in Fig. A2. It was identified, along with many other patterns from similar regions, with the phase $MgAl_2O_4$, having the f c c structure with $a = 0.808$ nm. Confirmation of the presence of oxygen was obtained using EELS.

MgO

MgO (periclase), which is f c c with $a = 0.421$ nm, was observed in the form of small precipitates (~ 50 nm diameter) in an amorphous reaction zone in annealed specimens, as shown in Fig. 5b. The phase took the form of fine crystals, normally associated with an amorphous phase that contained oxygen. Such regions tended to exhibit irregular porosity. Crystal structure identification was carried out using selected-area diffraction, which gave ring patterns; a comparison of the measured and calculated interplanar spacings is shown in Table AI. EDX analysis showed the crystals to contain more magnesium than the amorphous material, but an unambiguous analysis of each phase could not be carried out, owing to overlap.

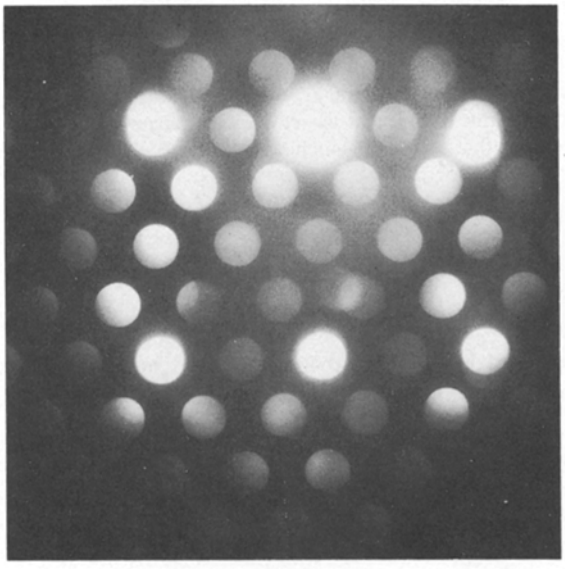

Figure A2 Bulk composite, heat treated 2 h at 650 °C; CBED pattern from an interfacial precipitate of magnesium spinel, [1 1 0] zone axis.

TABLE AI Comparison of interplanar spacings, *d*, from magnesium-rich crystals, measured using selected-area diffraction, with calculated values for MgO (periclase)

Indices (*h k l*)	*d* (nm)	
	Measured	Calculated
1 1 1	0.247	0.243
0 0 2	0.211	0.210
0 2 2	0.149	0.149
1 1 3/2 2 2	0.122	0.121/0.127
1 3 3	0.095	0.097

EELS spectra from such areas always showed the presence of oxygen. It is concluded that these regions consisted of crystals of MgO in an amorphous matrix which may have consisted mainly of Al_2O_3, although the presence of some dissolved magnesium cannot be ruled out.

Fe/Si/Al intermetallics

The main intermetallics present in the aluminium matrix of all composites were shown by EDX analysis to contain aluminium, silicon, chromium and iron with low levels ($\sim 1\%$) of manganese and copper. Many CBED patterns (e.g. Fig. A3a) were obtained in low-order zone axis orientations and identified according to a b c c structure with $a = 1.255$ nm, corresponding to the α' phase, nominally given in the literature [24, 30] as $(FeM)_3Si_2Al_{15}$, where M is Cr.

Quantitative analysis using particles that passed right through the thin foils gave varying compositions, according to the location of the particles and the heat treatment. The main uncertainty in the quoted compositions rests with the aluminium concentration, owing to possible interference from spurious X-rays, originating from the entire TEM specimen [27]. Essentially, three kinds of particles were identified:

1. a low (~ 0.5 at %) chromium phase (Fig. A3b) in the form of relatively large particles ($\gtrsim 1$ μm diameter), with approximate composition Fe_2SiAl_8, which were present at the fibre/matrix interfaces and grain boundaries;
2. a high chromium phase (Fig. A3c), present as small particles within the matrix of the as-processed bulk composite and certain heat-treated tow material, approximately $FeCrSi_2Al_{10}$; and
3. an intermediate chromium phase, seen in the matrix of heat-treated bulk samples, with approximate composition $Fe_2CrSi_2Al_{18}$.

A comparison of these findings with either the nominal composition or that of (approximately) Fe_2SiAl_{10} given by Skjerpe [32] from microprobe data indicates that this phase actually exists over a wide range of stoichiometry. It appears, in general, that the α' phase may be a prominent component of aluminium alloys in the 6000 series.

In addition to the α' phase, occasional observations were also made of a phase designated in the literature [30] as βFeSiAl. However, it proved impossible to

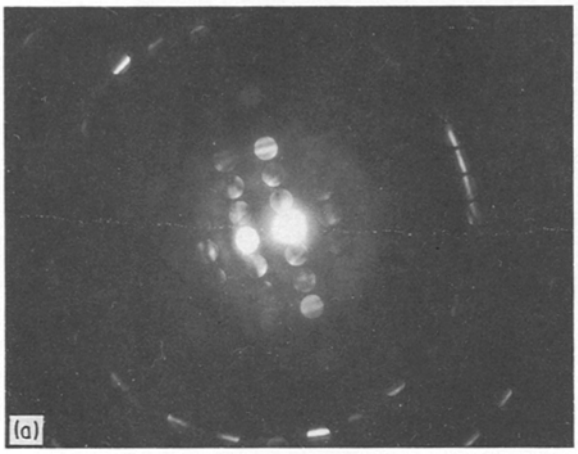

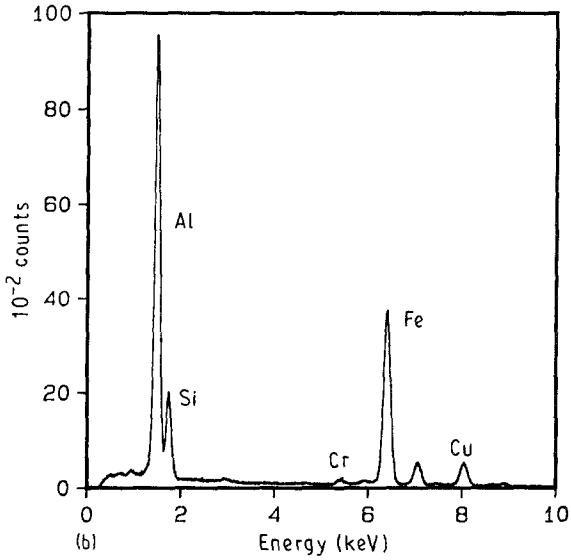

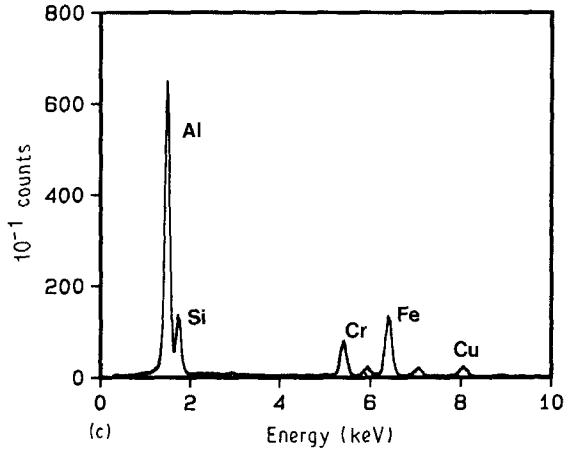

Figure A3 Characterization of the α'FeSiAl phases in the as-processed bulk composite: (a) CBED pattern, [1 3 0] zone axis; (b) EDX spectrum, low-chromium phase at a fibre/matrix interface; (c) EDX spectrum, high-chromium matrix precipitates.

describe the CBED patterns properly in terms of the designated monoclinic crystal structure [33]. This has resulted in a reassessment of the unit cell, which showed it to be B-face centred orthorhombic, with parameters $a = 0.6185$ nm, $b = 0.6251$ and $c = 2.069$ nm. The composition of this phase, as given by EDX analysis, was approximately $Fe_3Si_2Al_{10}$, with manganese and nickel as impurities at the ~ 1.5 at % level. Full details of this derivation will be published elsewhere [34].

Silicon

Precipitates of elemental silicon were observed in the bulk composite material and in tow specimens, following heat-treatment at 580 and 600 °C. They were invariably twinned and exhibited a strong Si*K* peak in EDX spectra, with an additional aluminium contribution that came either from excitation of the bulk sample or, in some cases, from matrix overlap. The identity of the phase was confirmed by CBED (Fig. A4) and also using EELS, from particles that passed right through the thin foil, where only a weak oxygen edge from the surface oxide film was present in addition to the silicon signal.

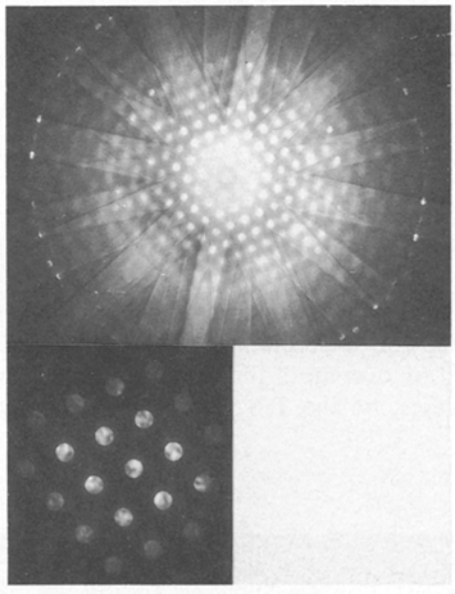

Figure A4 CBED pattern from elemental silicon in the as-processed bulk composite; [1 1 0] zone axis.

"Quaternary" phase

Intermetallics containing magnesium, aluminium, silicon, nickel and copper, with traces of iron and manganese, were occasionally observed in specimens of the wire tow, heat-treated at 580 °C, and in the as-processed bulk material. They were typically ~ 1 μm diameter and were present in the aluminium matrix, nucleated at the fibre interfaces. EDX analysis (Fig. A5a) indicated a composition close to $Mg_3Si_6Al_9(Ni_{1.3}Cu_{0.7})$ with 1.5 at % Fe and 0.5 at % Mn as impurities. Several CBED patterns (e.g. Fig. A5b) were indexed according to the "quaternary" phase, nominally $Mg_3Si_6Al_8Fe$, having a hexagonal cell with parameters $a = 0.663$ nm, $c = 0.794$ nm [30]. The diffraction patterns were similar to those expected from the αFeSiAl phase, but with many reflections missing.

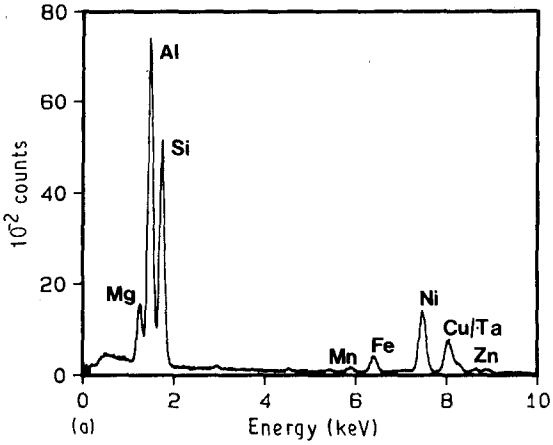

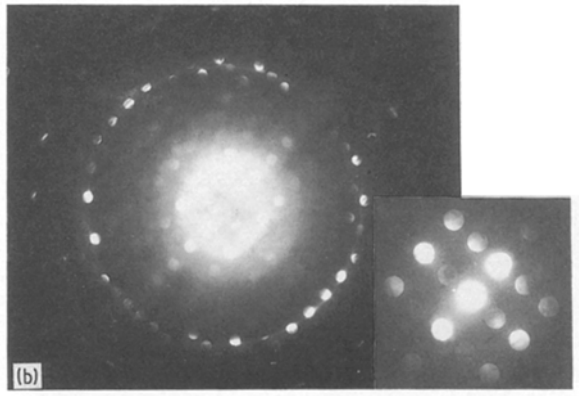

Figure A5 Identification of the "quaternary" intermetallic phase in a tow specimen, heat-treated 2 h at 580 °C: (a) EDX analysis; (b) CBED pattern, [0 1 $\bar{1}$ 2] zone axis.

This is a result of the near integral ratios between the lattice parameters and suggests a simple relationship between the atom positions in these two hexagonal phases. The atomic ratios of the elements magnesium, silicon and aluminium correspond well within the experimental accuracy with those given in the literature. However, the relative proportion of (Ni + Cu) is about twice that quoted for the quarternary containing iron.

$TiAl_3$

Occasionally, precipitates containing titanium were observed in specimens from heat-treated material. They were typically ~ 0.5 μm diameter. CBED patterns (e.g. as shown in Fig. A6) could be indexed in accordance with the intermetallic $TiAl_3$, which is body centred tetragonal with $a = 0.385$ nm and $c = 0.858$ nm. Quantitative EDX analysis was complicated by overlap of the aluminium matrix and, in some cases, by the TiB_x interlayer. Some particles appeared to contain chromium, dissolved at a level of a few atomic per cent, although it is possible that this observation may be a result of segregation of chromium to the fibre/matrix interface region.

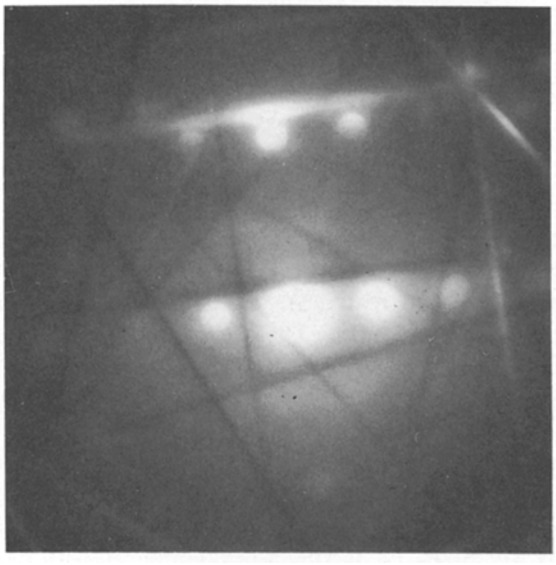

Figure A6 CBED pattern from a large $TiAl_3$ precipitate, formed at a fibre/matrix interface in a bulk composite, heat-treated 2 h at 700 °C; [1 1 2] zone axis.

References

1. R. J. PEPPER, J. W. UPP, R. C. ROSSI and E. G. KENDALL, *Met. Trans. ASM* **2** (1971) 1.
2. P. W. JACKSON, D. M. BRADDICK and P. J. WALKER, *Fibre Sci. Technol.* **5** (1972) 219.
3. V. C. NARDONE and J. R. STRIFE, *J. Mater. Sci.* **22** (1987) 592.
4. W. C. HARRIGAN Jr and D. M. GODDARD, in "International Conference on Composite Materials", Geneva, Switzerland edited by W. C. Harrigan, Jr, F. R. Strife and A. K. Dhingra. (AIME TMS Publication, Warrendale, PA, 1975) p. 849.
5. A. A. BAKER, C. SHIPMAN and P. W. JACKSON, *Fibre Sci. Technol.* **5** (1972) 213.
6. S. KOHARA and N. MUTO, in "International Conference on Composite Materials V", San Diego (1985) p. 631.
7. G. BLANKENBURG, *J. Austral. Inst. Metals* **4** (1969) 236.
8. S. J. BAKER and W. BONFIELD, *J. Mater. Sci.* **13** (1978) 1329.
9. I. H. KHAN, *Met. Trans. A* **7A** (1976) 1281.
10. M. KH. SHORSHOROV, T. A. CHERNYSHOVA and L. I. KOBELEVA, in "International Conference on Composite Materials IV", Tokyo (edited by T. Hayashi, K. Kawata, and S. Umekawal Japan Soc. for Composite Materials, Tokyo 1982) p. 1273.
11. M. MOTOKI and A. OKURA, *ibid.*, p. 1281.
12. J. J. TRILLET, L. TERTIAN and M. BENNET-GROS, *Les. Mem. Sci.* **57** (1960) 845.
13. *Idem., Mem. Sci. Rev. Met.* **62** (1960) 848.
14. P. W. JACKSON, D. M. BRADDICK and P. J. WALKER, *Fibre Sci. Technol.* **5** (1972) 219.
15. W. C. HARRIGAN Jr and W. W. FRENCH, Report ATR-75 (9450)-2, Aerospace Corp., El Segundo, CA, March 10, 1975.
16. X. LI, H. ZHANG and R. WU, in "International Conference on Composite Materials V", San Diego edited by W. C. Harrigan Jr, F. R. Strife and A. K. Dhingra (AIME TMS Publication, Warrendale, PA, 1985) p. 623.
17. A. OKURA, E. NAKATA and S. SAKAI, *J. Jpn Inst. Metals* **47** (1983) 249.
18. X. Q. CHEN and G. X. HU, in "Interfaces in Polymer, Ceramic and Metal Matrix Composites", edited by Hatsuo Ishida (Elsevier, New York, 1988) p. 381.
19. M. F. AMATEAU, *J. Compos. Mater.* **10** (1976) 279.
20. T. ERTURK, J. A. CORNIE and R. G. DIXON, in "Interfaces in Metal Matrix Composites", Cleveland, OH, edited by A. K. Dhingra and S. G. Fishman (AIME, Warrendale, PA, 1986) p. 239.

21. Y. SAWADA and M. G. BADER, in "First European Conference on Composite Materials", Bordeaux, edited by A. R. Bunsell, P. Lamicq and A. Massiah (European Association for Composite Materials, 1985) p. 577.
22. A. OKURA and K. MOTOKI, *Compos. Sci. Technol.* **24** (1985) 243.
23. S. D. TSAI, M. SCHMERLING and H. L. MARCUS, *Ceram. Engng Sci. Proc.* **2** (1981) 798.
24. L. F. MONDOLFO, in "Aluminum alloys: Structure and Properties" (Butterworths, London, 1976) pp. 534, 759.
25. H. ASANUMA and A. OKURA, *J. Jpn Inst. Metals* **48** (1984) 1198.
26. S. H. LO, S. DIONNE, G. J. C. CARPENTER and D. ZIMCIK, in "Interfaces in Metal-Ceramics Composites", edited by R. Y. Lin, R. J. Arsenault, G. P. Martins and S. G. Fishman (AIME, The Minerals, Metals and Materials Society, Warrendale, PA, 1990).
27. D. B. WILLIAMS, "Practical Analytical Electron Microscopy" (Philips, Mahwah, New Jersey, 1984) p. 60.
28. H. NAYEB-HASHEMI and J. SEYYEDI, *Met. Trans.* **20A** (1989) 727.
29. L. F. ALLARD, S. P. RAWAL and M. S. MISRA, *J. Metals* **38** (1986) 40.
30. J. E. HATCH (ed.), "Aluminum, Properties and Physical Metallurgy" (ASM, Ohio, 1984) p. 30.
31. T. MALIS and J. M. TITCHMARSH, in "EMAG-85" (The Institute of Physics, 1985) p. 181.
32. P. SKJERPE, *Met. Trans.* **19A** (1987) 189.
33. G. PHRAGMEN, *J. Inst. Metals* **77** (1950) 489.
34. G. J. C. CARPENTER and Y. LEPAGE, to be published.

Received 26 November 1990
and accepted 10 April 1991